Integrated Geophysical Investigation for Tin ore mineralization in parts of Kafanchan, middle Benue Trough, Nigeria.

ABSTRACT

By combining the results of the two geophysical techniques in parts of Gidan Waya Kafancha Kaduna State, numerous linear structures, possibly veins harbouring ore mineralisation, were discovered. These veins have varying electrical characteristics, some being conductive and others being non-conductive. Furthermore, certain veins are conductors within a resistive host, whereas others are located within a conductive host. The research region had approximately 30 conductive bodies(veins), most of which trended north-south direction and ranged in length from less than 25 meters to more than 150 meters. These discovered veins were shown on mineral prospecting maps. After careful consideration, 30 locations were chosen for the prospective ERT/IP survey generated from the EM-VLF, and 25 drilling points were derived from the ERT/IP dataset obtained from the inversion model, which is the priority drilling point.

Keywords: Tin ore, Very Low Frequency-EM, Electrical Resistivity Tomography/Induced Polarization, Kafanchan

1.0 Introduction

A geophysical investigation for Tin mineralization in Gidan Waya, Kaduna state, Nigeria was carried out to identify the abnormal area(s) that could be explored for Tin. Since Tin has little or no diagnostic geophysical signature, efforts should be geared toward using geophysical data as an indirect tool for its zone of mineralization to identify likely structural and geologic features favourable to mineralization.

Very Low Frequency Electromagnetic (VLF-EM) methods were used in the survey as an indirect approach to map the linear structural features like veins, fractures and contacts which act as conduits and hosts for ores (McNeill, 1980) and fracture zones (Olatunji, 1999). The advantages of the very low frequency electromagnetic (VLF-EM) method is that the technique is very rapid, can cover a wide area and is cost

The survey included Very Low Frequency Electromagnetic (VLF-EM) approaches as indirect techniques to indicate linear structural features such as veins, fractures, and contacts, which serve as conduits and hosts for ores (McNeill, 1980) and (Olatunji, 1999). The advantage of the very low frequency electromagnetic (VLF-EM) method is that VLF is well responsive to linear features: fracture, fault, vein, contact, attenuation of the VLF field is very slow, so

energization will be almost uniform throughout the entire area, VLF is sensitive to subtle conductivity variations and the method is fast and therefore saves time and cost (Fischer et. al., 1983; McNeill & Labson, 1991 and Bayrak, 2002).

In addition to the VLF-EM, the Induced polarization method was also used to complement or check if they are chargeable bodies of the result of the VLF-EM method. The combination of the two methods proved very useful in delineating priority targets for the exploitation of ore mineralization within the area.

Conversely, the very low frequency electromagnetic (VLF-EM) prospecting method is suited for analysing structural details and shallow subsurface conductors (Fisher et al., 1983) because it is not only quick but also cost-effective. VLF-EM is a passive approach that exploits EM frequency from military navigation radio transmitters operating in the VLF band (15–30 kHz) as the principal EM field. These stations situated around the world generate signals utilised for a range of applications, including groundwater detection and contamination evaluation, soil engineering, archaeology, and mineral prospecting for mapping narrow mineralized fault zones (Philips and Richards, 1975; Wright, 1988). The VLF-EM method also has been employed in mapping weathered layers in granitic terrain (Poddar and Rathor, 1983) and in the discovery of weak conductors possibly induced by water-filled fractures or shallow faults in nuclear waste management programs (Hayles and Sinha, 1986). For groundwater investigation, the VLF-EM approach has been demonstrated to be highly effective in contrast with vertical electrical sounding in hard rock terrains (Sundararajan et al., 2007). Hence, the VLF-EM approach is a popular EM tool for fast mapping of near-surface geo-logic structures (Philips and Richards, 1975; Parker, 1980; Saydam,1981). The theory of the VLF-EM technique is widely detailed in the literature (Paterson and Ronka, 1971; Philips and Richards, 1975; Wright, 1988; McNeill and Labson, 1991; Hutchinson and Barta, 2002). In the far-field above a uniform earth, the ground wave of the vertically polarized radio wave contains three field components: a radial horizontal electric field, a vertical electric field, and a tangential magnetic field. When these three fields hit electrically conducting ore deposits in the subsurface, eddy currents are created, causing the secondary fields to radiate outward from these conductors. Although this range is quite low for radio transmission, it is higher than that employed in normal low-frequency (1–3kHz) electromagnetic geophysical procedures. Paal (1965) recognised that radio waves at VLF

frequencies might be utilised to prospect for conductive mineral deposits. Since then, VLF transmitters situated around the world are being employed frequently as electromagnetic sources for near-surface geology mapping as an inductive survey approach. The VLF-EM approach has been frequently employed over the last three decades to image shallow subsurface structural characteristics of diverse importance. However, the analysis of reported VLF-EM anomalies is generally carried out utilising anomaly curves and nomograms (Kaikkonen, 1979; Saydam, 1981). Filtering utilising the methodologies of Fraser (1969) and Karous and Hjelt (1983) and subsequent contouring of the observed responses are the most typical practice to get qualitative information about the subsurface. VLF-EM has constrained probing depth capabilities, depending on the resistivity of the rocks and how they react to shallow bodies (Watson et al., 2001; Zou et al., 2022). The electrical resistivity method involving electrical resistivity tomography (ERT) has been successfully applied in different mineral exploration projects (Alile et al., 2017; Arwech et al., 2020; Horo et al., 2020; Olenchenko and Osipova, 2022) and environmental studies (Pierwoła, 2015; Benyassine et al., 2017; Gabarron et al., 2020; Olenchenko et al., 2020). The induced polarisation (IP) approach monitors changes in the chargeability of earth materials (Sumner, 2012; Zhdanov, 2018; Dusabemariya et al., 2020). This approach has wide applications in mineral exploration (Dembicki, 2016; Evrard et al., 2018; Prakash et al., 2018; Zhdanov, 2018; Dusabemariya et al., 2020).

2.0 Location and Accessibility

The research area is in Gidan Waya, southern Kaduna state, Nigeria, between $9^0$29'32'N and $9^0$29'08'N and $8^0$22'35'E and $8^0$22'16'E. The location of interest is roughly 1km by 1km. The geography is primarily undulating with rocky hills and flat plains. Figure 1 indicates elevation from 640m to 700m above sea level. Its top is 700m above sea level. The discharge is dendritic. Seasonal rivers and rivulets flow from mountains to flooded lowlands during the rainy season. The research area has Saharan and Atlantic air masses. The North Saharan air mass is dry and continental, while the South Atlantic air mass is cool, damp, and humid. These air masses generate dry and rainy seasons. The middle to the end of April heralds the beginning of perennial rains which finishes late October to early November. The highest rainfall is usually experienced in August. The harmattan, which starts in late December, is the coldest time with temperatures ranging between 20 °C and 30 °C. The hottest season is in April with temperatures climbing beyond 35 °C. The climate of the area is tropical humid

with roughly eight (8) months of wet season and four months or less of dry season. The vegetation is guinea savannah with primarily shrubs and very large trees appearing densely mostly along river channels.

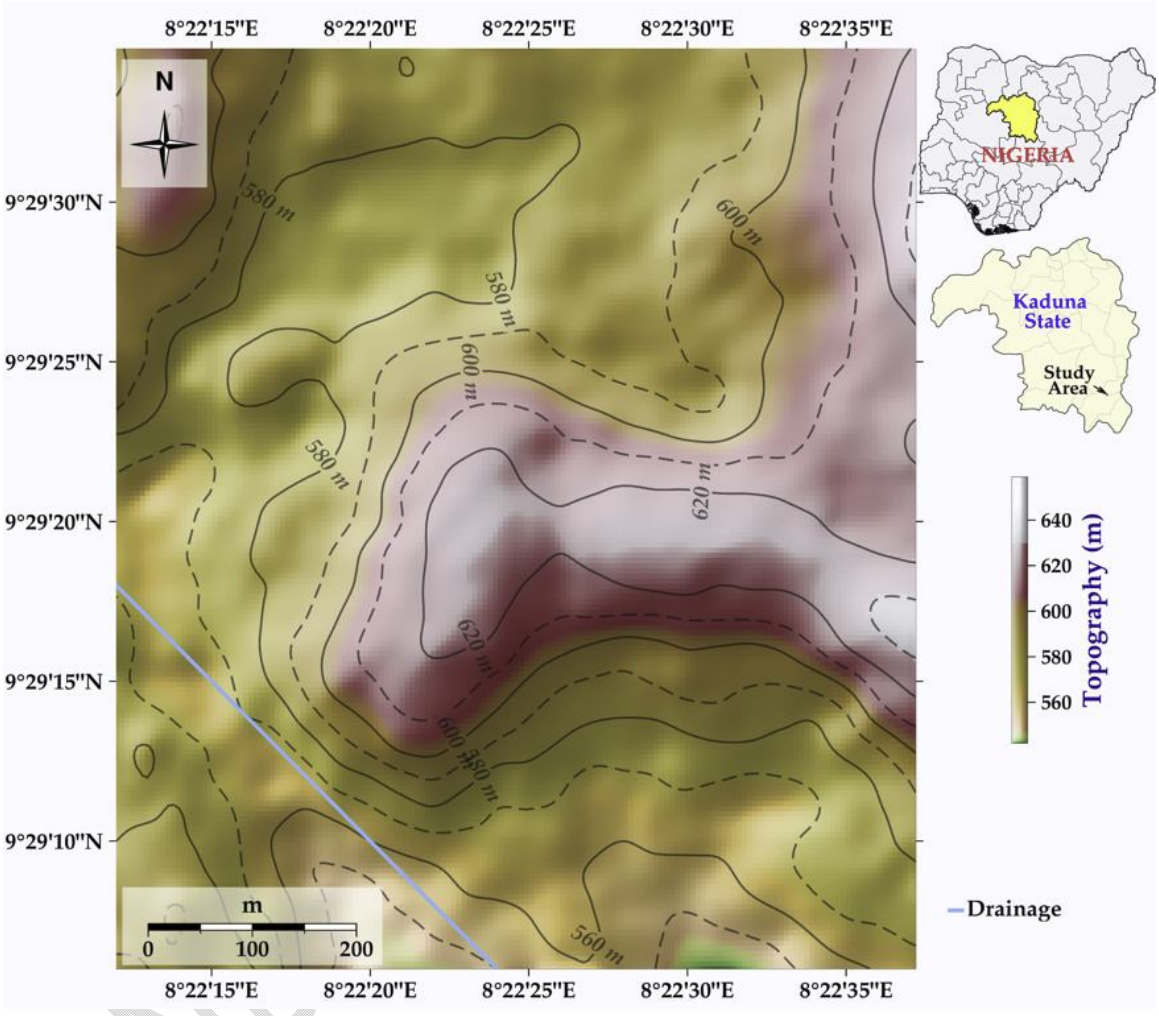

Figure 1: Location and Topography map of the study area

2. 1 Local Geology of the study area

The geology of Gidan Waya, Kafanchan is defined by the Precambrian Basement Complex (figure 2.), consisting of migmatites, gneisses, basalt, Coarse-grained porphyritic biotite and biotite hornblende granite, which is overlain by sedimentary rocks of the Cretaceous and Tertiary eras. These sedimentary rocks include sandstones, shales, and limestones. Additionally, pegmatites and quartzites are common, and often linked with the Basement Complex rocks (Obaje, 2009).

The soil in the area is typically sandy, with some places having clayey soils. The area is rich in mineral reserves, including tin, mica, columbite, iron ore, and gold. The groundwater potential is moderate to high, with boreholes and wells dipping into worn and cracked Basement Complex rocks and sedimentary aquifers. The landscape is moderately undulating, encompassing hills and valleys, giving a diverse atmosphere.

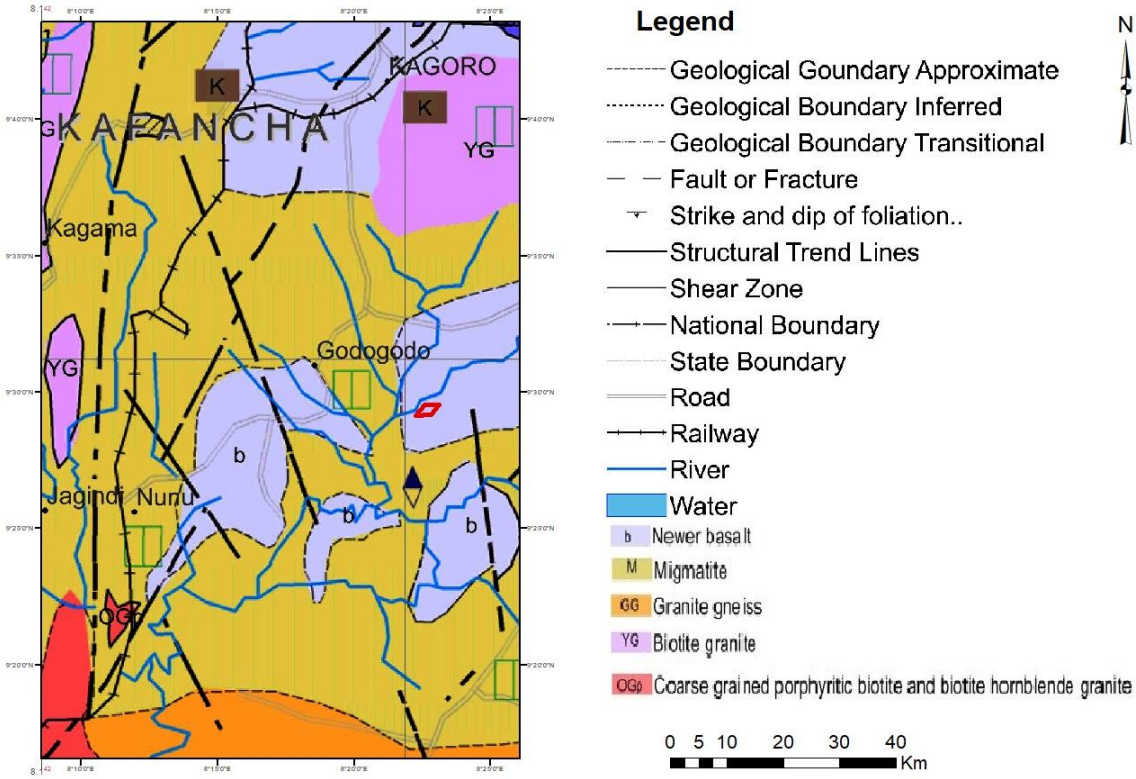

Figure 2: Geological map and Mineral Resources Map with the Study Area in Red Rectangle (Modified after NGSA, 2023)

2.2 Tin Mineralization in Nigeria.

Tin mineralization in Nigeria is concentrated in five key regions:

1. Jos Plateau: Significant tin deposits are found in the Jos, Bukuru, and Vom areas.

2. Bauchi State: Tin deposits occur along the Bauchi-Borno axis, including the Bauchi, Tafawa Balewa, and Bogoro areas.

3. Plateau State: Additional tin deposits are present in the Wase and Langtang areas.

4. Nasarawa State: Tin deposits are found in Nasarawa-Eggon and Akwanga areas.

5. Taraba State: Tin deposits occur in the Taraba-Bali and Gashaka areas.

Tin mineralization in Nigeria is commonly associated with:

1. Pegmatites: Coarse-grained granitic rocks containing tin-bearing minerals like cassiterite (SnO2).

2. Alluvial deposits: Tin is also found in streams and rivers.

3. Hydrothermal veins: Tin mineralization occurs in hydrothermal veins, often with quartz and sulfide minerals.

Primary tin-bearing minerals found in Nigeria include:

1. Cassiterite (SnO2)

2. Stannite (Cu2FeSnS4)

3. Staninite ((Cu,Fe)SnS2)

Several studies and reports have confirmed the presence of tin mineralization in the Kafanchan area, including:

1. Nigerian Geological Survey Agency (NGSA) reports of tin deposits in Kafanchan.

2. A 2014 Journal of Mining and Geology study identified tin mineralization in the Kafanchan-Saminaka area, with cassiterite (SnO2) as the primary tin-bearing mineral.

3. A 2019 study in the International Journal of Scientific Research in Environmental Sciences reported tin concentrations in soil and stream sediments in Kafanchan, indicating potential for tin mineralization.

The tin mineralization in Kafanchan is often associated with pegmatites and alluvial deposits, similar to other tin-producing areas in Nigeria.

3.0 Materials and Methods

3.1 VLF-EM Principles of operation

VLF is an excellent surveillance geophysical instrument for mapping geo-electric characteristics (Olorunfemi *et al.* 2005). It may be used wherever electric conductivity disparity is present between geological units. This may include fault and fracture mapping, groundwater studies, overburden mapping, pollution mapping and mineral exploration (Olatunji, 1999). Electrically conductive features tend to be more conductive than the underlying bedrock or host rock e.g. fault zones of mineralization, clayey or fine-grained soils etc.

VLF techniques measure the disturbances in a plane wave radio signal (15-30 KHz) emerging from one of the numerous worldwide radio transmitters used for submarine communications. VLF falls in the broad group of electromagnetic (EM) geophysical approaches.

The primary field (the transmitted radio signal) causes eddy currents to be induced in conductive geologic units or structures. Faraday's concept of electromagnetic induction explains that any oscillating magnetic field (e.g. the radio wave) will produce an electric field and thus an electric current in a conductive media. Those eddy currents in turn form a secondary magnetic field which is recorded by the VLF receiver.
The secondary or the disturbed field may be phase-shifted and orientated in a different direction from the Primary field depending on the form or geometry of the conductor, the orientation of the conductor and the conductivity contrast with the surrounding materials (e.g. the host rock). The device measures both the primary (in-phase) and the secondary (quadrature) fields concurrently. All VLF sensors measure two components of the magnetic field or "the tilt angle" and the ellipticity of the field.

The VLF-EM study leverages signals from VLF broadcasting stations globally. For optimal resolution, the orientation of the potential conductor should be perpendicular to the direction of wave propagation from the VLF station. As most mineralized veins have a NNE-SSW or N-S orientation, VLF stations with similar orientations are picked. In this survey, signals from Lualualei (23.4kHz), Le Blanc, France (18.3kHz), Bordeaux, France (15.1kHz), Annapolis, 21.4kHz, NW Cape, Australia, 22.3kHz and Cutler, Maine (24.0kHz) were used, with the best signal (23.4kHz) chosen for interpretation.

Twenty-eight (28) profiles were covered in the survey region utilising GEM GSM-19V portable VLF equipment. Data was stored on the instrument and eventually sent to a

computer via a configured downloading connection, then saved in an Excel Spreadsheet for easy management. Typical data from EM (VLF) is provided in Table 1. Quality Control (QC) and Quality Assurance (QA) were then applied to the raw data by visual inspection.

Table 1: A VLF-EM Database of one of the lines

Easting	Northing	Elevation	Frequency	In Phase	Quadrature	Field Strength	Time	Mid-Easting	Filtered Real
431345.2	1049070	593	23.4	0	-34.9	0.1	102946		
431356.8	1049073	591	23.4	-1.2	-14.8	0.1	103018		
431368.1	1049076	590	23.4	2.4	-31.7	0.1	103053	431362.5	-3.9
431379.1	1049072	590	23.4	-7.5	-15	0.1	103122	431373.6	-12.4
431381.6	1049070	590	23.4	-3.7	-16	0.1	103248	431380.4	0.2
431397.9	1049067	590	23.4	-1.2	-32.5	0.1	103309	431389.8	10
431406.2	1049068	589	23.4	0	-28	0.1	103338	431402	13.2
431415.8	1049069	588	23.4	8.3	-30.9	0.1	103408	431411	4.6
431424.9	1049067	589	23.4	-4.9	-16	0.1	103434	431420.3	-19.3
431438.7	1049071	589	23.4	-6.1	-17.2	0.1	103500	431431.8	-5.9
431450.5	1049074	590	23.4	3.6	-29.2	0.1	103528	431444.6	5.9
431459.2	1049074	592	23.4	-8.7	0	0.1	103601	431454.8	-8.6
431470.4	1049078	596	23.4	-2.4	-23.4	0.1	103720	431464.8	-2.3
431482.4	1049073	596	23.4	-5	-21.2	0.1	103751	431476.4	4.9
431493	1049073	597	23.4	-1.2	-10.9	0.1	103813	431487.7	11
431502.2	1049071	597	23.4	4.8	-18.2	0.1	103841	431497.6	20.5
431510.6	1049070	599	23.4	9.5	-25	0.1	103912	431506.4	8.3
431523.6	1049073	602	23.4	2.4	-13.4	0.1	103946	431517.1	-10.7
431534.7	1049070	605	23.4	1.2	-12.3	0.1	104014	431529.2	-8.3
431545.4	1049068	607	23.4	2.4	-14.6	0.1	104042	431540	2.4
431557.8	1049072	610	23.4	3.6	-29.2	0.1	104109	431551.6	-2.4
431568.6	1049071	614	23.4	-2.4	-22.2	0.1	104151	431563.2	-8.4
431580.7	1049073	615	23.4	0	-14.8	0.1	104226	431574.7	-3.7
431593	1049073	616	23.4	-2.5	-11.2	0.1	104300	431586.9	5.9
431604.4	1049073	618	23.4	6	-23.1	0.1	104325	431598.7	3.5

431615.4	1049073	618	23.4	-5	-21.5	0.1	104353	431609.9	-10.9
431626.1	1049070	619	23.4	-2.4	-28	0.1	104419	431620.8	-8.3
431637.1	1049069	619	23.4	-4.9	-22.2	0.1	104452	431631.6	-3.6
431648.3	1049069	620	23.4	-6.1	-3.7	0.1	104518	431642.7	-3.8
431660.3	1049070	622	23.4	-5	-11.2	0.1	104540	431654.3	7.2
431670.1	1049073	622	23.4	1.2	-28	0.1	104608	431665.2	17.1
431677.4	1049070	622	23.4	4.8	-26.8	0.1	104631	431673.7	7.4
431689.3	1049067	623	23.4	-1.2	-15	0.1	104651	431683.4	-10.9
431697.3	1049072	623	23.4	-3.7	-13.7	0.1	104713	431693.3	-14.8
431706.3	1049071	623	23.4	-7.5	-16.2	0.1	104742	431701.8	-12.6
431717.2	1049071	624	23.4	-10	-13.7	0.1	104805	431711.7	1.2
431730.8	1049069	625	23.4	0	-25.9	0.1	104831	431724	16.3
431740.9	1049072	625	23.4	-1.2	-30.4	0.1	104856	431735.9	8.8
431751.4	1049072	628	23.4	0	-34.1	0.1	104921	431746.1	-6.3
431763.9	1049073	631	23.4	-7.5	-18.7	0.1	104941	431757.6	-12.6
431773.8	1049069	631	23.4	-6.3	-10.1	0.1	105007	431768.8	-4.9
431783.2	1049071	633	23.4	-6.1	-13.5	0.1	105030	431778.5	6.5
431794.1	1049071	635	23.4	-1.2	-25.6	0.1	105053	431788.7	1.2
431804.7	1049073	637	23.4	-10	-15	0.1	105121	431799.4	-11.3
431814.1	1049075	637	23.4	-8.6	-17.2	0.1	105146	431809.4	8.6
431825.1	1049070	638	23.4	6	-31.3	0.1	105214	431819.6	30.6
431841.9	1049070	637	23.4	6	-21.6	0.1	105234	431833.5	1.2
431850.6	1049072	637	23.4	-7.4	-9.8	0.1	105259	431846.3	-19.4
431862.8	1049072	636	23.4	0	-26.8	0.1	105321	431856.7	-2.3
431875.3	1049073	635	23.4	-3.7	-20.9	0.1	105350	431869	1.3
431883	1049073	634	23.4	-2.4	-24.3	0.1	105418	431879.2	-4.9
431898.8	1049074	631	23.4	-6.2	-10	0.1	105506	431890.9	2.3
431908.5	1049071	627	23.4	2.4	-30.4	0.1	105546	431903.7	14.6
431917.7	1049072	624	23.4	3.6	-31.7	0.1	105617	431913.1	4.9
431927.8	1049072	622	23.4	-2.5	2.5	0.1	105646	431922.7	-9.7
431937.7	1049072	621	23.4	-1.2	-28	0.1	105722	431932.7	-3.4
431949.2	1049071	622	23.4	-1.1	-29.7	0.1	105747	431943.4	3.7
431960.6	1049071	621	23.4	1.1	-32.1	0.1	105811	431954.9	-4

431971.4	1049072	620	23.4	-7.4	-17.2	0.1	105842	431966	-9.8
431984.3	1049072	621	23.4	-2.4	-14.8	0.1	105910	431977.9	3.9
432001.2	1049072	620	23.4	0	-30.4	0.1	105938	431992.8	3.8
432012.4	1049073	620	23.4	-6	-17	0.1	110003	432006.8	-11
432024	1049072	618	23.4	-7.4	-2.4	0.1	110031	432018.2	-5.1
432035.8	1049073	615	23.4	-3.7	-35.8	0.1	110057	432029.9	17
432045.5	1049072	613	23.4	7.3	-21.9	0.1	110119	432040.7	7.2
432055.4	1049073	610	23.4	-11.2	-8.7	0.1	110147	432050.4	-14.8
432064	1049071	607	23.4	0	-18.2	0.1	110212	432059.7	7.4
432077.8	1049071	602	23.4	3.5	-29.7	0.1	110252	432070.9	11.1
432087.3	1049068	598	23.4	-3.6	-28	0.1	110318	432082.5	-3.5
432097.5	1049071	597	23.4	3.6	-27.7	0.1	110344	432092.4	14.2
432106.5	1049073	593	23.4	10.5	-38.8	0.11	110420	432102	5.7
432111.5	1049075	590	23.4	-4.8	-34.1	0.1	110521	432109	-14.1
432124.2	1049073	584	23.4	4.8	-23.1	0.1	110550	432117.9	-0.9
432134.8	1049075	583	23.4	0	-23.4	0.1	110637	432129.5	2.4
432147	1049072	577	23.4	2.4	-19.5	0.1	110708	432140.9	-16.1
432159.4	1049070	575	23.4	-13.7	-13.7	0.1	110757	432153.2	-18.5
432168.7	1049073	571	23.4	-2.4	-25.9	0.1	110837	432164.1	54
432178.8	1049067	570	23.4	45.1	1.6	0.46	110920	432173.8	60
432187.3	1049070	568	23.4	-1.2	-24	0.1	111013	432183.1	-43.9
432197	1049072	565	23.4	0	-9.8	0.1	111050	432192.1	-48.9

3.3 ERT/IP-Field Operations

A 2D electrical resistivity tomography (ERT) survey, commonly known as imaging, was undertaken utilising a Geomative GD-10 Supreme Geoelectrical system, produced by ST Geomative Co. Ltd., China. The system comprises of a meter that simultaneously monitors subsurface resistivity and chargeability, powered by an external alternating source electric generator. By connecting the components with several electrodes, the system allows 2D imaging of the subsurface's electrical characteristics over multiple layers as illustrated in Figure 3 and Figure 4.

The survey encompassed 28 profile lines, each roughly 300 meters long. Using a double dipole electrode design, electrical resistivity and IP tomography were measured consistently over each profile, with an inter-electrode spacing of 10 meters. Multiple electrodes were utilised to record data, providing extensive information on the subsurface's electrical properties which were then analysed and evaluated using Res2Dinv software. This enabled for a detailed understanding of the subsurface's electrical characteristics and structure.

4.0 Data Processing and Interpretation

4.1 EM-VLF Data Processing

In the VLF-EM survey, one of the elements affecting the measured tilt angle and ellipticity data is the effect of topographic (ranging from 640m to 700m) relief in steep locations. Uneven terrain provides major abnormalities which lead the measured VLF data to vary from the pattern which would be expected on flat ground. Terrain adjustment was not carried out because the area examined is rather flat.

The in-phase and quadrature components of the vertical field were shown for qualitative interpretation. This is to observe signatures of comparable features replicating a certain geological structure.

Fraser filter was applied on the genuine components of the vertical field. This filter calculates horizontal gradients and smoothens the data to offer maximum values over conductors. As suggested by Fraser (1969), the shape of an anomaly along a profile can be convolved using a four-point filter expressed as F2,3 = (H3+H4) – (H1+H2) This is plotted midway between the H2 and H3 stations. This filter operator changes every true cross-over or inflexion point of the real component anomaly to positive peaks while the peak becomes negative. The map of filtered real components (Figure 3) was also constructed to indicate the scope of the true conductive targets in the area.

4.1.1 Interpretation of the VLF-EM Survey Data

The interpretation of the VLF-EM profiles and maps was qualitative/semi-quantitative. The qualitative interpretation involved the inspection of profiles and maps for signatures or patterns diagnostic of the target of interest or the use of the characteristic features of the

anomaly curve (e.g. inflection or cross-over point or peak positive and peak negative amplitude of anomaly curves) to locate the top of the target.

A typical North-South VLF-EM real component anomaly across an inclined contact, vein or approximation of a thin conductor is S-shaped with the negative amplitude shoulder showing on the northern flank. The inflection point of such an anomaly is positioned immediately on top of the contact or conductor if it is vertically dipping. The inflection point is somewhat moved towards the down-dip side if the body is gradually dipping. In this scenario, the anomaly is asymmetrical and the anomaly shoulder (+ve or -ve amplitude) is highest on the down-dip side (Olorunfemi et. al., 2005).

The semi-quantitative interpretation involves a 2-D inversion of the real component anomaly curves using the IXVLF program to compute an effective penetration depth. From stacked plots of In-phase versus Quadrature as shown in (Figure 4 and 5), the cross-over points are most definitely representing the top of conductive substances. These entities, suspected to be mineralized veins all trend averagely and roughly in the North-South direction (Figures 4 and 5). In the subject area, these plots revealed many parallel lineaments presumed to represent fractures or fissures with conductive in-fillings. The Filtered Real map (Figure 3) when viewed revealed highly intriguing and potential features. There are several noticeable conductivity anomalies in the area, stretching virtually N-S continuously, especially in the central part of the research area. Some of these structures nonetheless display very low conductivity indicative of very resistant materials. Interestingly, all these structures trend in the N-S direction, similar with the known mineralized structural trend of the geological zone with a minor departure in some cases. It can be noted in most profiles that the amplitude of the in-phase is always bigger than that of the quadrature at that position, which shows that the anomaly is presumably a conductive target.

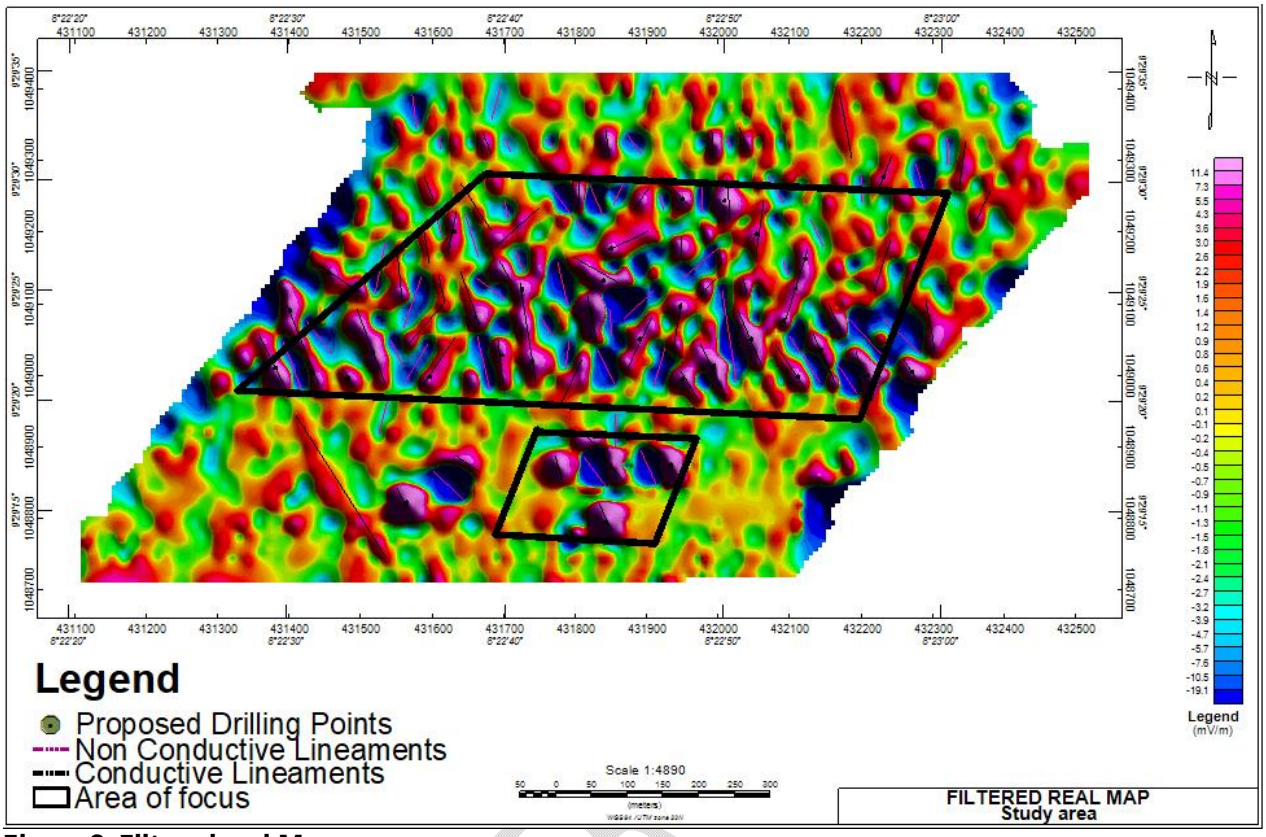

Figure 3: Filtered real Map

Figure 4: In phase, quadrature and filtered real of Ln15_18.2khz

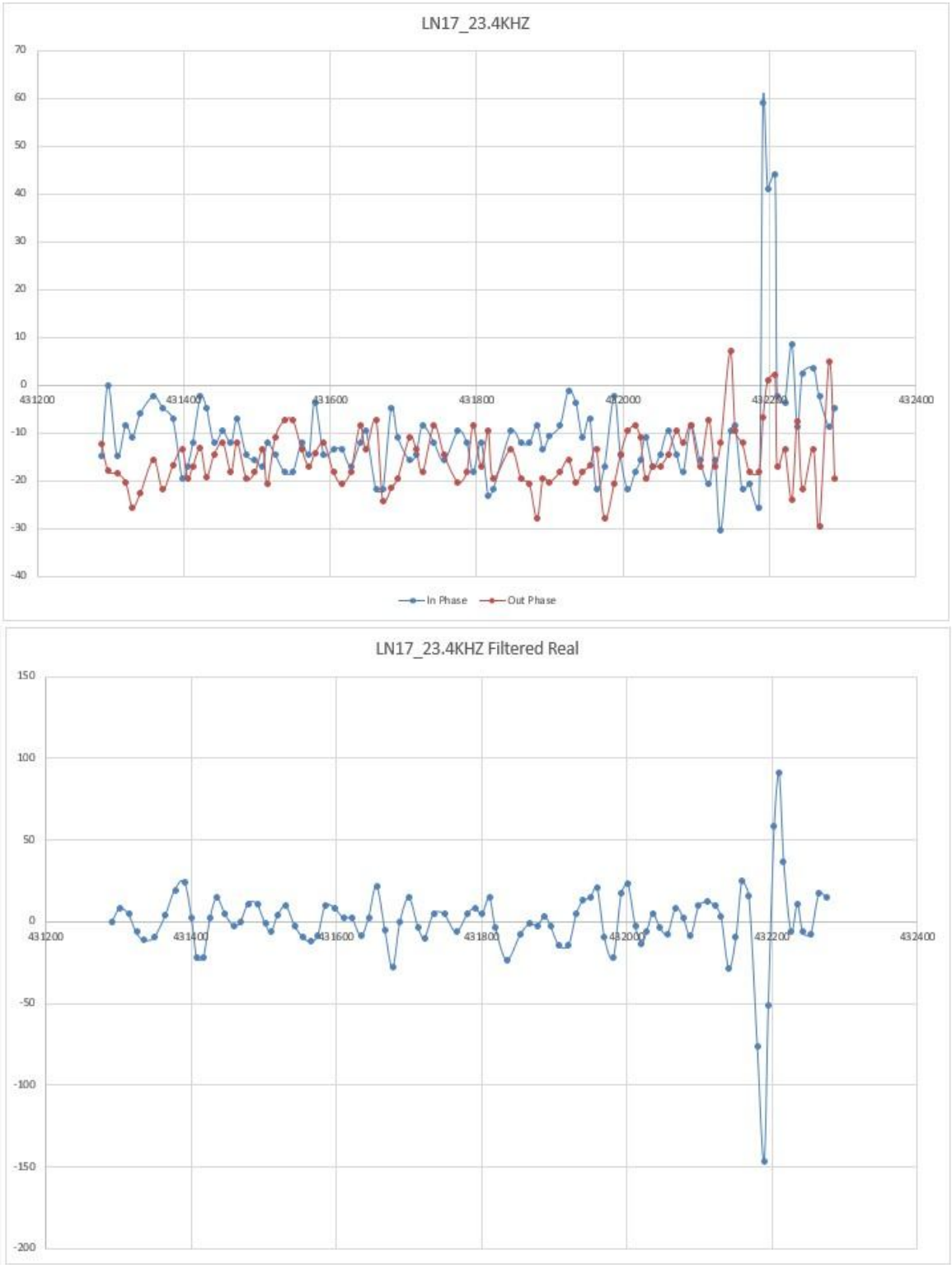

Figure 5: In phase, quadrature and filtered real of Ln17_23.4khz

4.2 Interpretation of the ERT/IP Survey Data

The IP (Induced Polarization) survey uses a pair of non-polarizing electrodes to inject current into the subsurface (Clement, 2021). When the current was quickly shut off, the primary voltage (V) between another pair of non-polarizing potential electrodes did not return to zero but plummeted to a secondary voltage (Vs) that declined over time, producing an IP effect in the time domain. This consequence is perceived chargeability (Binley, 2015; Clement, 2021). The ERT/IP profiles were conducted in an east-west orientation, perpendicular to the overall trends of the veins derived using VLF-EM data.

Profile line IP1 indicated three possible mineralized zone of chargeable bodies with chargeability ranging from 15.3 to 45.2 mV/V and resistivity values ranging from 1716 to 5857 Ωm at depths of 25m, 40m, and 68m. Profile line IP2 indicated a medium to high chargeability anomaly body of 45.2 mV/V at 13m deep and a corresponding high resistivity value of 2633 Ωm, as well as two mineralized zones. Profile line IP3 exhibited the maximum chargeability of 112 mV/V at 13m deep and disseminated bodies of chargeability value of 30.2 mV/V and resistivity of 0.042 Ωm at 25m depth.

Profile line IP5 indicated one possible mineralized body with chargeability value of 0.675 mV/V and a high resistivity value of 22681 Ωm, as well as one mineralized zone. Profile line IP6 found four mineralized ore bodies of high chargeability values of 83.3 mV/V and resistivity values ranging from 441 to 1529 Ωm. Profile line IP7 featured two low resistivity and chargeability bodies of 16 mV/V and resistivity value of 188 Ωm. Profile line IP8 indicated disseminated ore bodies with chargeability value of 147 mV/V and associated resistivity value of 237 Ωm, as well as a low chargeable body of 0.037 mV/V and resistivity value of 58.6 Ωm at depths of 25m and 13m, respectively.

Profile line IP9 indicated pockets of anomalous bodies with chargeability values of 18.7 mV/V and 57.3 mV/V at depths ranging from 12.8m to 68m, accompanied by resistivity anomalies of 251 and 1340 Ωm. In contrast, profile line IP11 displayed a mineralized zone with a comparatively low resistivity value of 145 Ωm and a chargeability value of 12.7 mV/V. Additionally, a mineralized zone and disseminated ore with high chargeability (77.9 mV/V) were identified at depths between 25m and 57m.

Notably, profile line IP13 revealed a large chargeability anomaly towards the middle and end of the profile, characterized by a value of 78.9 mV/V and a resistivity of 4699 Ωm at depths of 25m and 57m. Furthermore, profile line IP15 revealed a significant chargeability anomaly of 105 mV/V, coupled by a resistivity value of 1139 Ωm at a depth of 25m.

Profile IP17 indicated one disseminated ore body with a chargeability value of 59.4 mV/V and a high resistivity of 35158 Ωm at a depth of 30m, as well as two mineralized zones at 39m with a chargeability value of 20 mV/V and a resistivity value of 43.2 Ωm. Profile IP18 showed relatively low chargeability and resistivity values of 21.2 mV/V and 86.2 Ωm at a depth of 25m, which could imply a Mica anomaly. Similarly, profile IP19 demonstrated a dispersed and mineralized zone at depths ranging from 13m to 40m, with a chargeability of 39.3 mV/V and a resistivity value of 175 Ωm.

Profile IP21 revealed a pocket of disseminated ore and a mineralized zone with chargeability values ranging from 27.7 mV/V to 129 mV/V and resistivity values spanning 52 Ωm to 4185 Ωm at depths between 25m and 40m. Profile IP27 demonstrated both mineralized zones and disseminated ore, defined by a chargeability value of 42.9 mV/V and a resistivity value of 1078 Ωm at depths ranging from 13m to 30m.

Profile IP28 exhibited pockets of disseminated ore with high chargeability values of 271 mV/V to 315 mV/V and a resistivity value of 146 Ωm at a depth of 40m. Notably, profile IP4 revealed a moderate resistivity value of 245 Ωm and a chargeability value of 33.8 mV/V at a depth of 40m, indicating the existence of disseminated sulphide ore, possibly Tin ore.

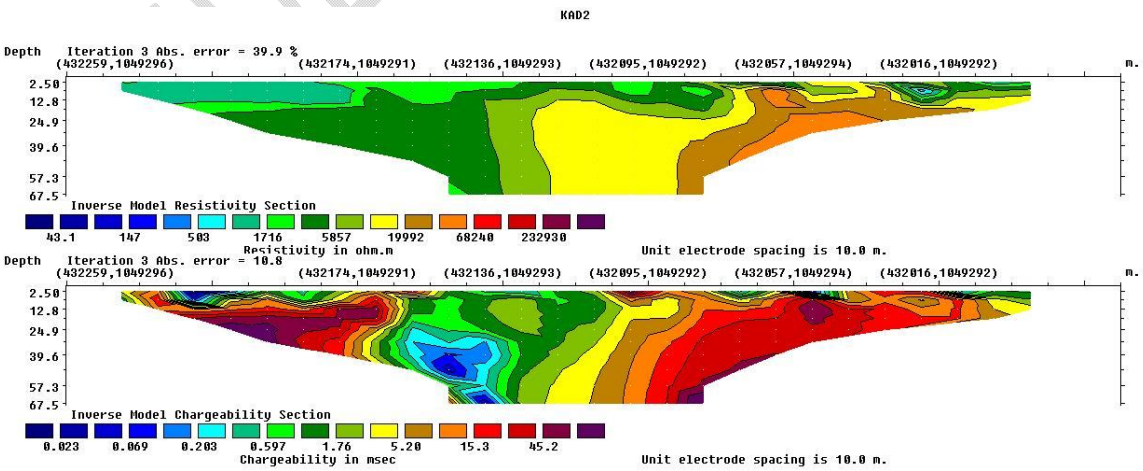

KAD2B

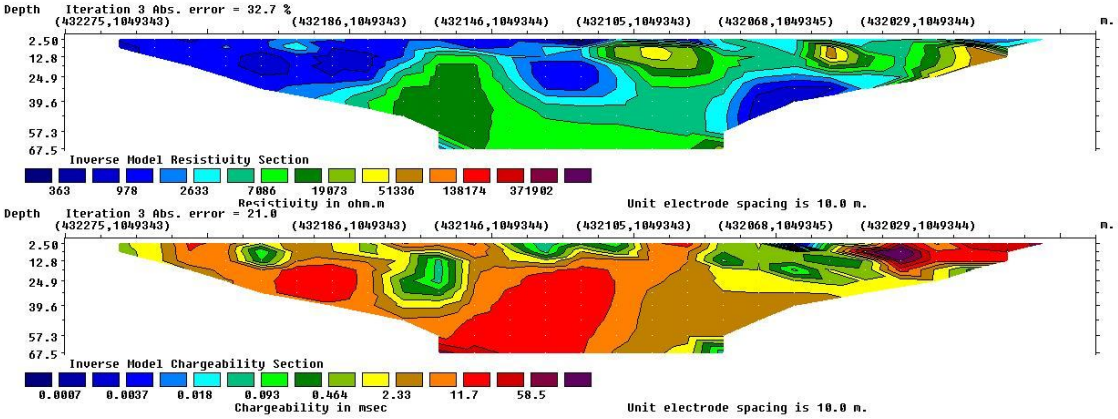

KAD6

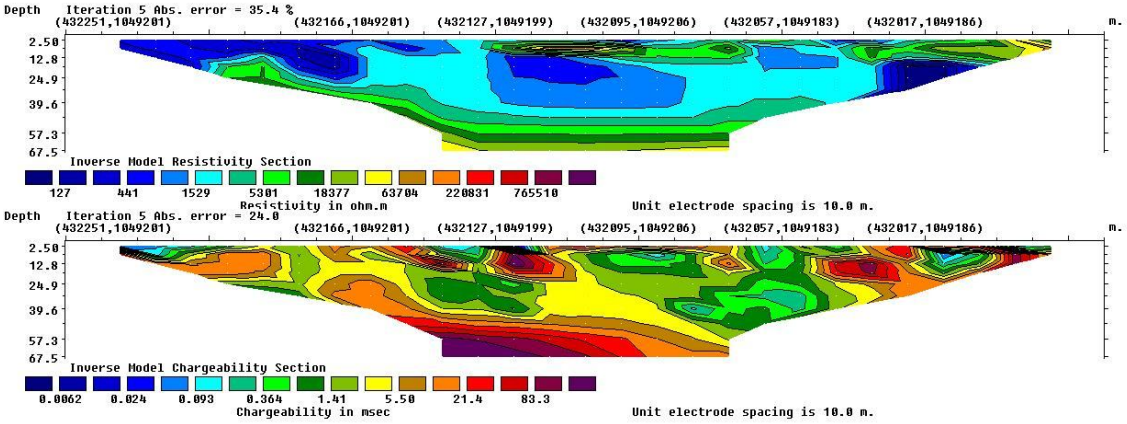

KAD9

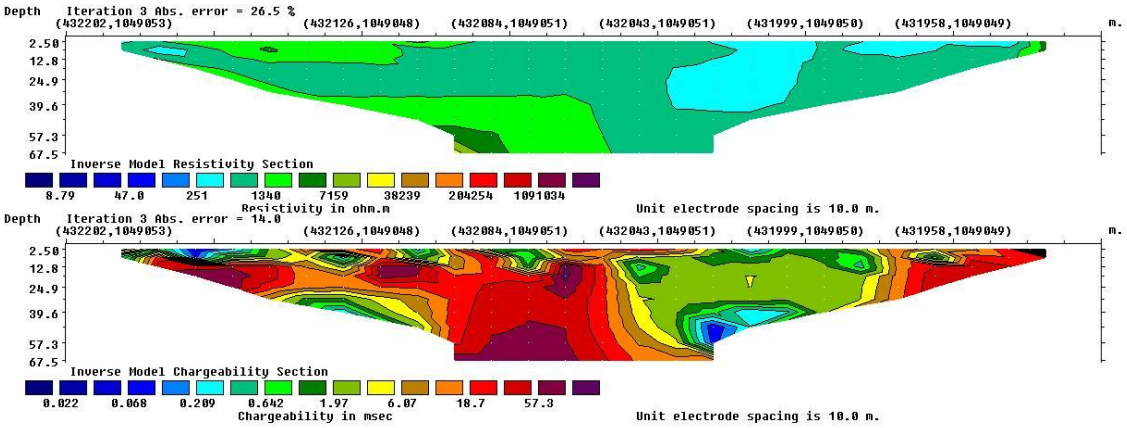

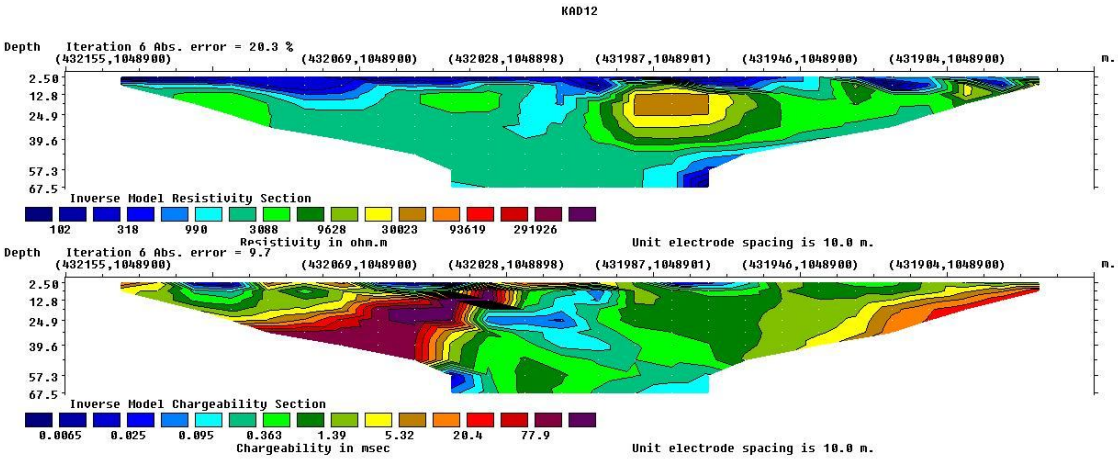

Figure 6: ERT/IP inversion model for the selected profiles (IP2, IP6, IP9, IP11 and IP12)

4.3 Discussion on the interpretation of VLF (EM) and ERT/IP

Combining the results of the two geophysical approaches, many linear structures presumably veins which are considered to house ore mineralization were detected. Some are conductive while others are not. Some are conductors within a resistive host whereas others are within a conductive host. Over 30 such veins trends predominantly N-S were discovered in the research area. Their length varies from less than 25m to more than 150m. The detected veins were placed on respective mineral prospective maps (Figure 7). Twelve (12) places for prospective core drilling were identified from these veins following a closer investigation (Table 2).

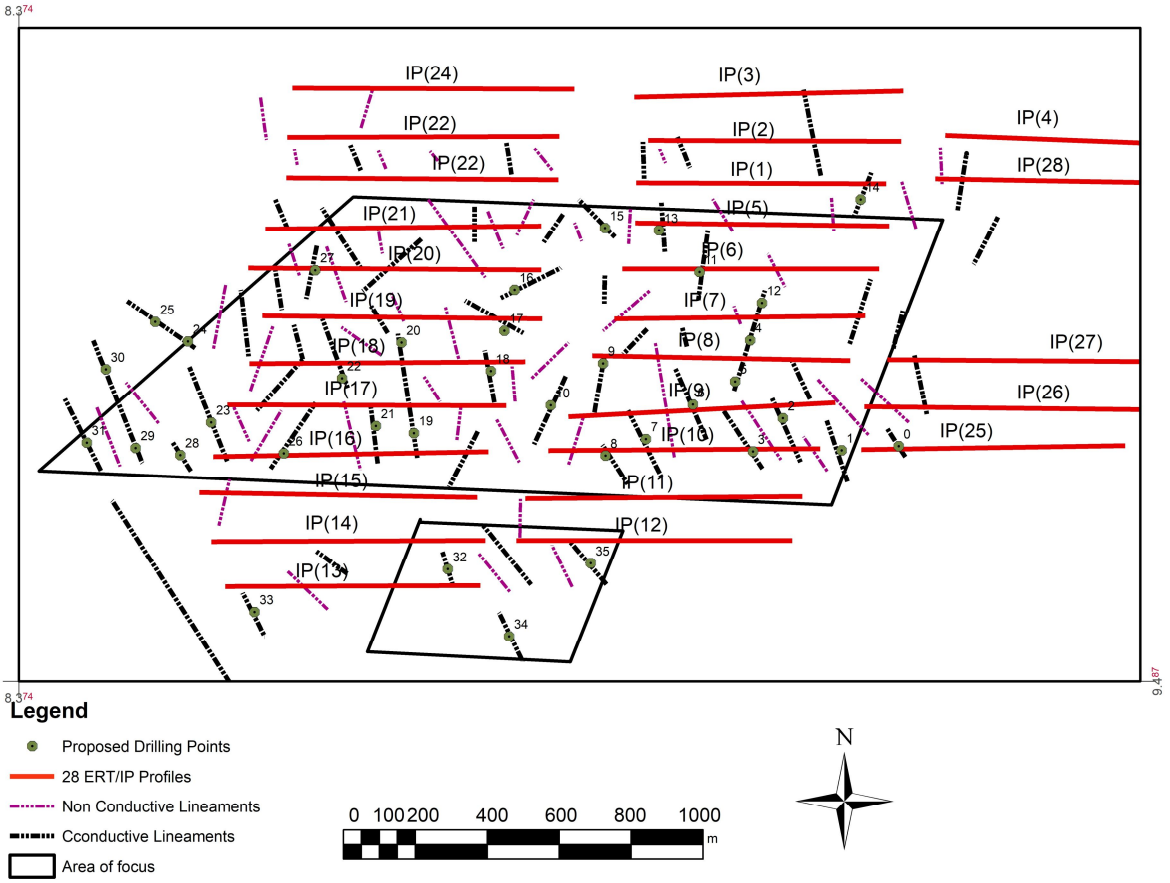

Figure 7: Mineral Prospective Interpreted Map

Table 2: Characteristics of the identified bodies (veins)

Profiles	Vein Trend	Vein Length	Depth(m)
IP2	NE-SW	Mineralized zone (20)	30
IP2	NE-SW	Mineralized zone (55)	68
IP2	NW-SE	Disseminated ore (20)	19
IP6	NW-SE	Disseminated ore (10)	15
IP6	NW-SE	Disseminated ore (50)	68
IP6	NW-SE	Disseminated ore (20)	28
IP9	NE-SW	Disseminated ore (40)	26
IP9	NE-SW	Disseminated ore (20)	18

IP9	NE-SW	Mineralized zone (60)	57
IP9	NE-SW	Disseminated ore (50)	68
IP11	NE-SW	Mineralized zone (50)	42
IP12	NE-SW	Disseminated ore (30)	25

4.4 Conclusion

From the findings of all the examinations carried out, a wide range of linear structures were discovered (Figures 3, 4, 5, 6, &7). Through thorough interpretation and technical examination of the general results, it can be determined that most of these structures are mineralized veins with varied degrees of characterisation. Their answers to physical factors also revealed that some are conductive while others are non-conductive. From the aforementioned, the following conclusions were consequently formed.

1. The research outlined several linear structures.
2. Most of these structures are conductive while some are non-conductive.
3. The majority of the features are presumed mineralized veins.
4. The depth models for selected areas of the target as shown from the SPI depth map revealed that these veins are near the surface within the range of 10 and 40m
5. Twelve (12) priority targets for core drilling are identified from the study area.

Disclaimer (Artificial intelligence)

Option 1:

Author(s) hereby declare that NO generative AI technologies such as Large Language Models (ChatGPT, COPILOT, etc.) and text-to-image generators have been used during the writing or editing of this manuscript.

Option 2:

Author(s) hereby declare that generative AI technologies such as Large Language Models, etc. have been used during the writing or editing of manuscripts. This explanation will include the name, version, model, and source of the generative AI technology and as well as all input prompts provided to the generative AI technology

Details of the AI usage are given below:

1.

2.

3.

Reference

Alile, O.M., Aigbogun, C.O., Enoma, N., Abraham, E.M., Ighodalo, J.E., 2017. 2D and 3D electrical resistivity tomography (ERT) investigation of mineral deposits in Amahor, Edo State, Nigeria. Niger. Res. J. Eng. Environ. Sci 2, 215–231.

Arjwech, R., Sriwangpon, P., Somchat, K., Pondthai, P., Everett, M., 2020. Electrical resistivity tomography (ERT) data for clay mineral mapping. Data Brief 30, 105494.

Bayrak M. (2002) Exploration of Chrome Ore in Southwestern Turkey by VLFEM. Jour of the Balkan Geophy Society 5: 35-46.

Benyassine, E.M., Lachhab, A., Dekayir, A., Parisot, J.C., Rouai, M., 2017. An application of electrical resistivity tomography to investigate heavy metals pathways. J. Environ. Eng. Geophys. 22 (4), 315–324.

Binley, A., 2015. Tools and techniques: electrical methods. In: Schubert, G. (Ed.), Treatise on Geophysics, second ed. Elsevier, pp. 233–259.

Clement, W.P., 2021. Geophysical site characterization. In: Alderton, David, Elias, Scott A. (Eds.), Encyclopedia of Geology, second ed. Academic Press, pp. 805–814.
Dembicki, H., 2016. Practical Petroleum Geochemistry for Exploration and Production. Elsevier, p. 751.

Dusabemariya, C., Qian, W., Bagaragaza, R., Faruwa, A., Ali, M., 2020. Some experiences of resistivity and induced polarization methods on the exploration of sulfide: a review. J. Geosci. Environ. Protect. 8, 68–92.

Evrard, M., Dumont, G., Hermans, T., Chouteau, M., Francis, O., Pirard, E., Nguyen, F., 2018. Geophysical investigation of the Pb–Zn deposit of Lontzen–poppelsberg, Belgium. Minerals 8 (6), 233.

Fisher, G., B.V. Le Quang, and I. Muller, 1983, VLF ground surveys, a powerful tool for the study of shallow two-dimensional structures: Geophysical Prospecting, **31**, 977–991.

Fraser, D. C., 1969, Contouring of VLF-EM data: Geophysics, **34**, 958–967.

Gabarron, M., Martínez-Pagan, P., Martínez-Segura, M.A., Bueso, M.C., Martínez- Martínez, S., Faz,

A., Acosta, J.A., 2020. Electrical resistivity tomography as a support tool for physicochemical properties assessment of near-surface waste materials in a mining tailing pond (El Gorguel, SE Spain). Minerals 10 (6), 559.

Hayles, J. G., and A. K. Sinha, 1986, A portable local loop VLF transmitter for geological fracture mapping: Geophysical Prospecting, **34**, 873–896.

Horo, D., Pal, S.K., Singh, S., Srivastava, S., 2020. Combined self-potential, electrical resistivity tomography, and induced polarisation for mapping of gold prospective zones over a part of Babaikundi-Birgaon Axis, North Singhbhum Mobile Belt, India. Explor. Geophys. 51 (5), 507–522.

Hutchinson, P. J., and L. S. Barta, 2002, VLF surveying to delineate long wallmine induced fractures: The Leading Edge, **21**, 491–493.

Kaikkonen, P., 1979, Numerical VLF modeling: Geophysical Prospecting, **27**, 815–834.

Kaikkonen, P., and S. P. Sharma, 1998, 2D nonlinear joint inversion of VLF and VLF-R data using simulated annealing: Journal of Applied Geophysics, **39**, 155–176.

Karous, M., and S. E. Hjelt, 1983, Linear filtering of VLF dip-angle measurements: Geophysical Prospecting, **31**, 782–794.

McNeill JD, and Labson VF (1991). Geological mapping using VLF radio fields. In Electromagnetic Methods in Applied Geophysics: Volume 2, Application, Parts A and B (pp. 521-640). Society of Exploration Geophysicists. https://doi.org/10.1190/1.9781560802686.ch7.

McNeill JD (1980). Electromagnetic Terrain conductivity measurement at low induction numbers (Tech. Note) TN-6, Geonics Ltd., Mississauga, Canada, 15pP.

Obaje N. G. (2009). Geology and Mineral Resources of Nigeria. Springer Verlag, Heidelberg (Germany), 240pp.

Olatunji S (1999). Geophysical Site Investigation of the Federal College of Education (F.C.E), Zaria, Nigeria Unpublished MSc. Thesis, A.B.U., Zaria.

Olenchenko, V.V., Osipova, P.S., Yurkevich, N.V., Bortnikova, S.B., 2020. Electrical resistivity dynamics beneath the weathered mine tailings in response to ambient temperature. J. Environ. Eng. Geophys. 25 (1), 55–63.

Olenchenko, V.V., Osipova, P.S., 2022. Electrical resistivity tomography of alluvial deposits during prospecting for placer gold. Russ. Geol. Geophys. 63 (1), 98–108.

Olorunfemi MO, Fatoba JO, Ademilua LO (2005). Integrated Vlf- Electromagnetic and

Electrical resistivity survey for groundwater in a crystalline basement complex terrain of southwest Nigeria. Global Journal of Geological Sciences 2005; 3(1):71-80

Paal, G., 1965, Ore prospecting based on VLF radio signals: Geoexploration,**3**, 139–147.

Parker, M. E., 1980, VLF electromagnetic mapping for strata bound mineralization near Aberfeldy: Transactions of the Institute of Mining and Metallurgy, Section B, **89**, B123–B133.

Paterson, N. R., and V. Ronka, 1971, Five years of surveying with the very low frequency electromagnetic method: Geoexploration, **9**, 7–26.

Philips, W. J., and W. E. Richards, 1975, A study of the effectiveness of the VLF method for the location of narrow-mineralized fault zones: Geoexploration, **13**, P.215–226.

Poddar, M., and B. S. Rathor, 1983, VLF survey of the weathered layer in southern India: Geophysical Prospecting, **31**, P.524–537.

Pierwoła, J., 2015. Using Geoelectrical imaging to recognize Zn-Pb post-mining waste deposits. Pol. J. Environ. Stud. 24 (5), 2127–2137.

Prakash, N., Enright, M., Angus, R., 2018. The effective use of forward modelling and petrophysical analyses in the application of induced polarisation surveys to explore for disseminated sulphide systems in the Paterson province, western Australia. ASEG Extended Abstracts 1, 1–8.

Saydam, A. S., 1981, Very low frequency electromagnetic interpretation using tilt angle and ellipticity measurements: Geophysics, **46**, 1594–1606.

Sundararajan, N., M. Narasimhachary, G. Nandakumar, and Y. Srinivas, 2007, VES and VLF an application to ground water exploration, Khammam, India: The Leading Edge, 708–716.
Sumner, J.S., 2012. Principles of Induced Polarization for Geophysical Exploration. Elsevier, p. 248.

Watson, K., Fitterman, D., Saltus, R.W., McCafferty, A., Swayze, G., Church, S., et al., 2001. Application of geophysical techniques to minerals-related environmental problems. In: Open file report (Ed.), US Geological Survey 1–458.

Wright, J. L., 1988, VLF Interpretation manual: Scintrex, Ltd.

Zhdanov, M.S., 2018. Foundations of Geophysical Electromagnetic Theory and Methods. Elsevier, p. 1722p.

Zou, H., Pei, Q.M., Li, X.Y., Zhang, S.T., Ware, B., Zhang, Q., et al., 2022. Application of field-portable geophysical and geochemical methods for tracing the Mesozoic-Cenozoic vein-type fluorite deposits in shallow overburden areas: a case from the Wuliji'Oboo deposit, Inner Mongolia, NE China. Ore Geol. Rev. 142, 104685.